Hindawi
International Journal of Chemical Engineering
Volume 2023, Article ID 2360674, 12 pages
https://doi.org/10.1155/2023/2360674

Research Article

Copper Selenide (CuSe) Monolith Fabricated by Facile Copper Foam Selenization for Efficient Photocatalytic Degradation of Methylene Blue

Yefan Wang, Shan Gao, Haoying Li, Yang Cao, Yijie Zhai, Niezheng Chen, and Zequn Yang

School of Energy Science and Engineering, Central South University, Changsha 410083, China

Correspondence should be addressed to Zequn Yang; zequn_yang@hotmail.com

Received 13 March 2023; Revised 9 August 2023; Accepted 11 September 2023; Published 26 September 2023

Academic Editor: Federica Proietto

A critical challenge that impedes the application of photocatalytic techniques for organic dye degradation from polluted industrial effluents is that traditional powdery photocatalysts exposed limited photo-absorption sites and exhibited inefficient recyclability. To overcome these challenges, this study designed a one-step process to synthesize a monolithic copper selenide (CuSe)-based photocatalyst. The characterization results fully supported that the maintenance of the copper foam during the selenization process was the prerequisite for the monolithic photocatalyst to keep its structural integrity in photocatalytic reactions. The surface of the monolithic photocatalyst fully covered by active CuSe is crucial for the exposure of photocatalytically active sites and the efficient degradation of methylene blue (MB). It was found that the CuSe-based monolithic photocatalyst exhibited excellent MB degradation performances under harsh pH conditions and high MB concentrations. From these perspectives, it is reasonable to conclude that the CuSe-based monolithic photocatalyst as prepared is a promising alternative to traditional powdery photocatalysts for organic dye degradation and industrial effluent cleaning.

1. Introduction

Severe water pollution caused by the release of synthetic dyes from industrial activities is one of the major environmental concerns in the 21st century [1]. According to documented estimations, the annual generation of synthetic dyes worldwide reaches approximately 7×10^5 tons with over 1,000 types [2]. Among the synthetic dyes generated, 15% of them are lost during the dyeing process and released into the ecosystem with textile effluents [3]. The aqueous reservoir colored and polluted by these organic dyes thus suffers harmful and uncontrollable eutrophication that significantly reduces its oxygenation capacity [4]. Besides, the bioaccumulation of these organic pollutants also damages aquatic life and eventually becomes a serious health threat to human beings. Upon ingestion, the adverse physical effects of synthetic dyes include but are not limited to nausea, diarrhea, vomiting, breathing difficulties, and gastritis infections [5]. From these perspectives, it is imperative to develop effective and efficient methods to degrade and remove these synthetic dyes from textile effluents and aquatic environment. Methylene blue (MB), as an extremely carcinogenic thiazine pollutant that has been widely used in various industries for different purposes (e.g., dyeing of cotton, wool, and fabrics; coloring of paper, as a hair coloring agent and redox reaction indicator in outer space, etc.), has received special attention during the technical development process [6, 7].

Although different techniques including adsorption [8], membrane filtration [9], coagulation/flocculation [10], ion-exchange removal [10], catalytic ozonation [11], and photocatalytic degradation [12] have been proposed as effective pathways for MB degradation, considering its chemical stability and the inherent complexity of MB-polluted sources, there is still not an omnipotent technique to achieve the removal of MB from all industrial processes.

Among the abovementioned techniques, photocatalytic degradation is known as one that possesses unique advantages such as the direct utilization of solar energy, the facile cyclic functionalization of photocatalysts, and the total mineralization of dyes. In addition, by purposefully manipulating the band gap of semiconductors, it is theoretically possible to achieve the rational degradation of target pollutants from aquatic environment, while keeping the residual properties of the aquatic environment generally unchanged. Such rationality can hardly be realized when other degradation techniques are adopted for organic dye removal. With these advantages, developing MB removal techniques based on photocatalytic degradation has been a vibrant research area in the past twenty years with the related international environmental standards becoming more stringent [13].

To further extend the applicability of photocatalytic techniques for organic dye degradation from polluted sources, the rational design and successful synthesis of efficient photocatalysts are highly desirable. Critical drawbacks suffered by traditional photocatalysts in powdery forms include (i) low absorption rate of light due to the shielding effects among powders, (ii) the ineffective exposure of active sites because of the agglomeration of nanoparticles, and (iii) the possible introduction of new pollutants into the aquatic system and the tedious process for photocatalyst recycling [14]. From these perspectives, developing a monolithic photocatalyst may be a feasible solution for the abovementioned challenges considering that (1) anchoring photocatalysts on monolithic substrates well-disperses active components, thus increasing the light absorption efficiency and optimizing the contact between pollutants and photocatalysts [15] and (2) the tedious recovery process of photocatalysts is skipped as they can be easily recycled together with the monolithic substrates [16]. These undeniable merits indicate that monolithic catalysts may be more practical and effective options for photocatalytic removal of organic dyes from the aquatic system.

However, although monolithic photocatalysts have long been recognized as potential alternatives to powdery ones for organic pollutant degradation from industrial sources, previous studies mainly developed monolithic photocatalysts based on traditional photocatalysts such as titanium dioxide (TiO_2) and zinc oxide (ZnO) with wide band gaps. Because they can only absorb light within the ultraviolet range that only accounts for 4-5% of solar irradiation, these photocatalysts exhibit relatively limited photocatalytic degradation performances under practical scenarios [17–21]. Besides, to fabricate monolithic TiO_2 and ZnO, a post-treatment strategy is generally adopted to load them on another monolithic supporter such as honeycomb or silicon dioxide via physical interactions [22, 23]. The unstable loading pattern makes it possible for the photocatalysts to be released into the aquatic system and cause secondary pollution. Finally, to enhance the photocatalytic performances of catalysts with wide band gaps, co-catalysts or heterocomponents are required to narrow their band gaps and enhance the absorption of light irradiation [24, 25], which inevitably increases the operation costs of the photocatalytic techniques. To overcome these critical challenges in the fabrication of monolithic photocatalysts, it is of great importance to design new strategies to synthesize effective monoliths for photocatalytic organic dye degradation from industrial sources.

Accordingly, in this work, a one-step procedure was developed to load copper selenide (CuSe) on the surface of copper foam to achieve the efficient photocatalytic degradation of MB. CuSe with an ideal band gap of 2.1–2.5 eV exhibits excellent absorption abilities for light in both ultraviolet and visible ranges [26, 27]. The in-situ growth fabrication process of CuSe ensures that the photocatalyst stably anchored on the copper foam substrate because of the formation of chemical interactions. By properly controlling the selenization time, the copper framework could be well-maintained during the selenization process, thus ensuring that the monolithic photocatalyst keeps its structural integrity in photocatalytic degradation. With these advantages, the CuSe-based monolithic photocatalyst prepared exhibited excellent MB degradation performances when its concentration was extremely high or the pH condition was harsh. From these perspectives, it is reasonable to conclude that the CuSe-based monolithic photocatalyst is a promising alternative to traditional powdery photocatalysts, which might further extend the applicability of the photocatalytic techniques for organic dye degradation and industrial effluent cleaning.

2. Experimental Methods

2.1. Photocatalyst Synthesis and Regeneration. The CuSe-based monolithic photocatalysts used in this work were prepared through a one-step selenization process (as shown in Figure 1). Typically, the commercial copper foam (>99.99%) was first cut into cubic pieces with the side length of 10 mm × 10 mm × 10 mm. Then, hydrochloric acid (HCl, Aladdin) solution with the concentration of 3 mol·L^{-1} was adopted to wash out any copper oxides on the surface of copper foam that had been stored in air. In a separate beaker, 0.002 mol of selenium powder (Se, Aladdin) was dissolved in 0.01 mol·L^{-1} sodium borohydride ($NaBH_4$, Aladdin) solution at 90°C until it totally turned transparent. Then, commercial copper foams with different densities (5 ppi, 10 ppi, and 20 ppi) were added into the Se-$NaBH_4$ solution with continuous stirring for 20 min. After the surface of the foams transformed into black, they were separated out from the solution, washed with deionized water/ethanol for several times, and dried at 100°C for 3 h to obtain the final monolithic photocatalysts. To regenerate the deactivated photocatalyst, the CuSe-based monolith was impregnated in hydrogen chloride (HCl, Aladdin) at 40°C for 2 min (the weight ratio between CuSe-based monolith and HCl equaled to 1 : 10). After the CuSe on the surface of copper foam was removed, the copper foam underwent a re-selenization process following the abovementioned procedure. Besides, to prepared powder CuSe photocatalysts, the same synthesis procedure was adopted without adding copper foam. Commercial P25 TiO_2 and ZnO powders were

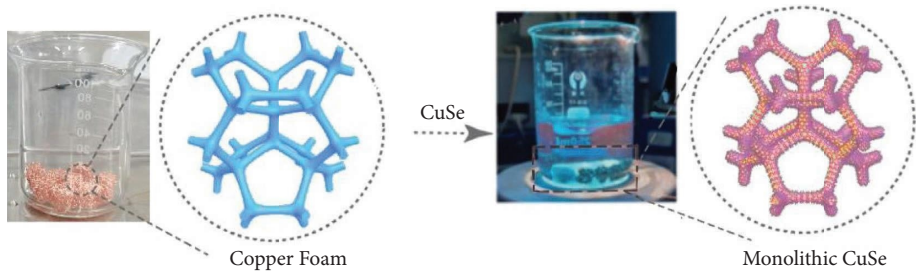

Figure 1: Diagrammatic illustration of the preparation procedure of CuSe-based monolithic catalysts.

purchased as reference photocatalysts to claim the efficiency of the CuSe-based monolith.

2.2. Photocatalyst Characterization. The crystallinity of the CuSe-based photocatalyst was measured by X-ray diffraction (XRD, D8 Bruker AXS, Germany) with two thetas from 10° to 80° in Cu_α ($\lambda = 0.154$ nm) radiation. The morphologies of the CuSe-based photocatalyst were recorded by a scanning electronic microscope (SEM, FEI F50, USA), during which the energy-dispersion X-ray (EDX) scanning and mapping were conducted to determine the composition content and distribution. A transmission electron microscope (TEM, JEOL 2100F, Japan) was used to determine the morphologies of the as-prepared CuSe-based photocatalyst. The CuSe as formed on the surface of monolithic copper foam was separated out before conducting the TEM and high-resolution TEM (HRTEM) tests. The primary goal was to identify the morphology and crystal phase of the CuSe as formed. The total organic carbon (TOC) change during the degradation process was tested based on a TOC analyzer (Germany, Analytik Jena AG). A 10-ppi copper foam, 5 pieces of $1 \times 1 \times 1$ cm of monolithic CuSe, 10 mg·L^{-1} of methylene blue, and a pH value of 7 were adopted to conduct the TOC analysis experiment.

2.3. Photocatalytic Performance Test. MB as a typical dye pollutant was adopted to test the photocatalytic performance of the CuSe-based monolithic photocatalysts. When performing the degradation tests, the monolithic photocatalysts were suspended in MB solution under continuous stirring. A 300 W Xe lamp was used to supply irradiation in both ultraviolet and visible range with the peak wavelength of 320 nm. The distance between the photoreactor and Xe lamp was fixed as 10 cm. During the testing process, the MB solution was continuously sampled with an interval of 5 min to draw the concentration change curves. The MB concentrations in each test were determined by an ultraviolet-visible (UV-vis) spectrophotometer at the wavelength of 525 nm. Before conducting the UV-vis test, the light absorption characteristics of the standard MB solutions with concentrations of 5, 10, 15, 20, and 25 mg·L^{-1} were first determined to draw the standard curve. As shown in Figure 2, when the concentrations of MB equaled to 5, 10, 15, 20, and 25 mgL^{-1}, the absorbance intensity of 525-nm light of the solutions were 0.58, 1.22, 1.81, 2.35, and 2.96, respectively. The correlation coefficient (R^2) of this standard

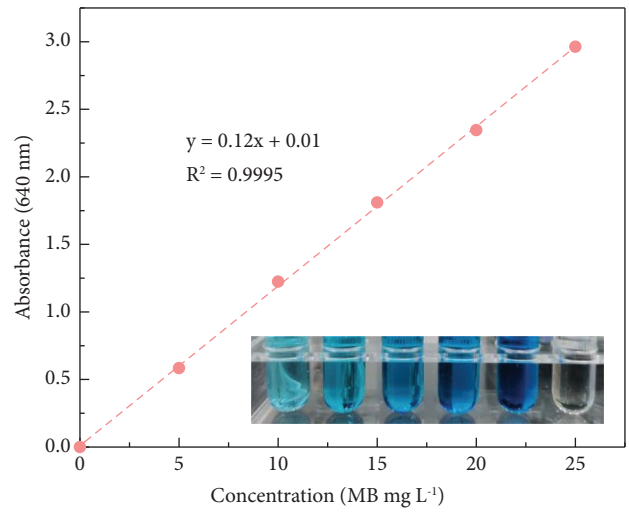

Figure 2: Concentration-absorbance curve as obtained based on the standard MB solutions (the standard curve shows a good linear relation of absorbance with MB concentration ($R^2 = 0.9999$).

curve reaching 0.9995 suggested its reliability to determine the specific MB concentrations under practical scenarios.

Based on the abovementioned testing procedures, to fully test the photocatalytic performances of CuSe-based monolithic photocatalysts, eight sets of experiments were conducted. The detailed experimental conditions are shown in Table 1 for reference. In particular, Set I experiment was designed to rule out the adsorption of MB on CuSe-based monolith under dark conditions. The MB degradation performances of different photocatalysts were compared in Set II experiments. Set III experiments tested the influence of the density of copper foams on the MB degradation performances of CuSe-based monolithic photocatalysts. Set IV experiment was dedicated to investigating the effects of photocatalyst dosage on the photocatalytic performance. The impacts of MB concentrations on the photocatalytic kinetics were determined in Set V experiment, and the influences of the pH value of the solutions were explored in Set VI experiment. Finally, Set VII and Set VIII experiments were conducted to test the recyclability and reusability of the CuSe-based monolithic photocatalysts.

3. Results and Discussion

3.1. Photocatalyst Characterization. Figure 3 shows the XRD pattern of the CuSe-based monolithic photocatalyst as prepared by a one-step selenization process. As shown, most

Table 1: Experimental conditions.

Experiments	Photocatalysts	Photocatalyst dosage (pieces)	MB concentration ($mg \cdot L^{-1}$)	pH value	Cyclic number
Set I	Monolithic CuSe (60-min dark experiment)	5	10	7	1
Set II	Monolithic CuSe Powder CuSe Commercial P25 Commercial ZnO	5	10	7	1
Set III	Monolithic CuSe (5, 10, and 20 ppi)	5	10	7	1
Set IV	Monolithic CuSe (10 ppi)	3, 5, 8, 10	10	7	1
Set V	Monolithic CuSe (10 ppi)	5	10, 15, 20, 25	7	1
Set VI	Monolithic CuSe (10 ppi)	5	10	3, 5, 7, 9, 11	1
Set VII	Monolithic CuSe (10 ppi)	5	10	7	10
Set VIII	Regenerated CuSe (10 ppi)	5	10	7	4

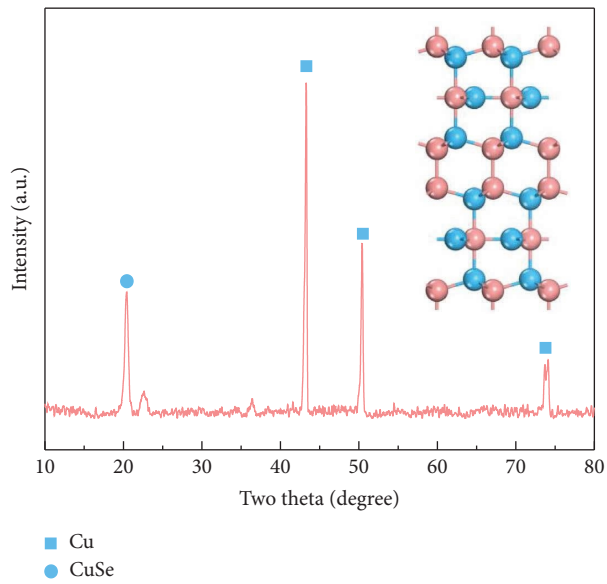

Figure 3: XRD pattern of the CuSe-based monolithic photocatalyst (inserted with the crystal structure of klockmannite).

of the peaks in the XRD pattern centering at approximately 43°, 50°, and 74° were attributed to elemental copper (JPCD #04-0836), which indicates that the structural integrity of the copper skeleton was generally maintained during the selenization process. Such excellent maintenance is indispensable for the CuSe-based photocatalyst to keep its monolithic structure instead of collapsing during the photocatalytic reaction process. Besides, it should be noted that, after selenization, there was a new peak that did not belong to elemental copper appear at around 20°. Through scrutinizing possible phases, it was found that this peak was ascribed to the (004) planes of klockmannite (JPCD #34-0171, the hexagonal phase of CuSe). The exposure of (004) planes is in line with the growth pattern of hexagonal CuSe (the structure is shown in the inserted figure of Figure 3), i.e., according to the classic BFDH (a model developed by Bravais, Freidel, Donnay, and Harker) model, the growth rate of the surfaces of a growing polygon was generally in inverse proportion to their lattice spacing. In CuSe hexagonal case, the lattice space between the (001) planes equaling to 1.74 nm is much larger than that between the (100) planes equaling to 0.34 nm, thus the planes along the (001) direction will grow much more slowly than the six energetically equivalent planes along the (100) directions. Hence, the CuSe tended to self-assemble into hexagonal phases with the exposure of the (004) planes [28, 29].

To further identify the morphology of the CuSe-based monolithic photocatalyst as prepared, its SEM images are shown in Figure 4. As shown in Figure 4(a), the CuSe-based monolithic photocatalyst well-kept its structural integrity during the photocatalytic reaction process, which further supported the critical role of the copper skeleton to maintain the monolithic architecture. Figures 4(b) and 4(c) demonstrate that, after selenization, the surface of the copper foam was covered by nanoparticles with diameters less than 1 μm, which was probably attributed to the formation of CuSe on copper foam surface. Increasing the resolution of the SEM image proved that the nanoparticles as formed on the surface of copper foam shaped in nanorod-like morphology. Compared to the previous studies, it was found that the coverage by these rod-like nanoparticles was not an inherent feature of copper foam [30–32]. Contrarily, pure copper foam was characterized by a relatively smooth surface with no rod-like nanoparticle accumulation. Thus, it is reasonable to conclude that the rod-like nanoparticles appeared on the surface of selenized copper foam formed during the selenization process.

To further explore the phase of the rod-like nanoparticles as formed on the surface of copper foam, the energy dispersive spectrometry (EDS) mapping patterns of the CuSe-based monolithic photocatalyst is shown in Figure 5. As shown in Figures 5(a) and 5(b), copper and selenium were homogenously dispersed on the surface of copper foam. The EDS mapping results that well-agree with the XRD pattern of the CuSe-based monolithic photocatalyst further suggested that the rod-like nanoparticles were CuSe. Besides, the compositional ratios of copper and selenium in the CuSe-based monolithic photocatalyst equaled to approximately 15% and 85% (as shown in Figure 5(c)), respectively. These compositional ratios indicate that most of the copper component in copper foam was kept unchanged during the selenization process, which is also in accordance with the XRD result. Therefore, an important conclusion can be drawn from such consistency, i.e., the selenization process this work adopted is reasonable enough to fully cover the surface of selenized copper foam with abundant heterocomponents, while its skeleton structure ensuring that the monolithic photocatalyst should not collapse during the photocatalytic reaction process, which was well-maintained due to the residual copper phase.

Finally, to confirm the phase of the rod-like heterocomponents as formed on the surface of copper foam, TEM tests were conducted in this work. As shown in Figure 6(a), after separating the nanoparticles from the surface of copper

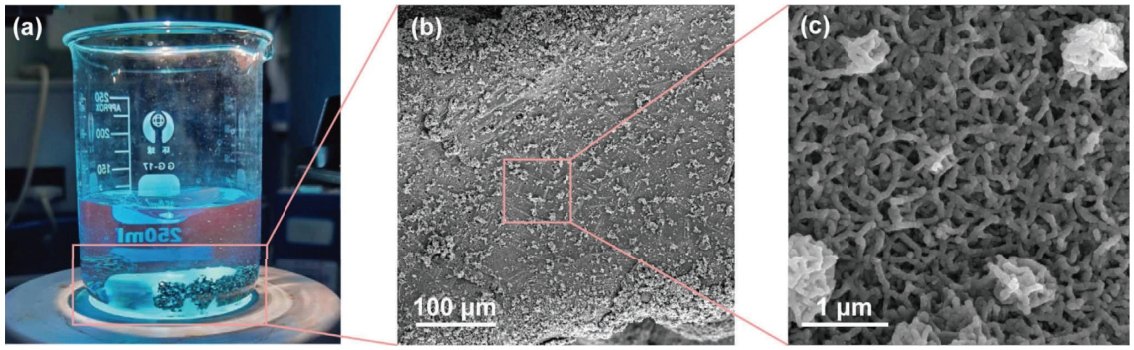

Figure 4: (a) The CuSe-based monolithic photocatalyst as prepared and (b, c) SEM images of the CuSe-based monolithic photocatalyst.

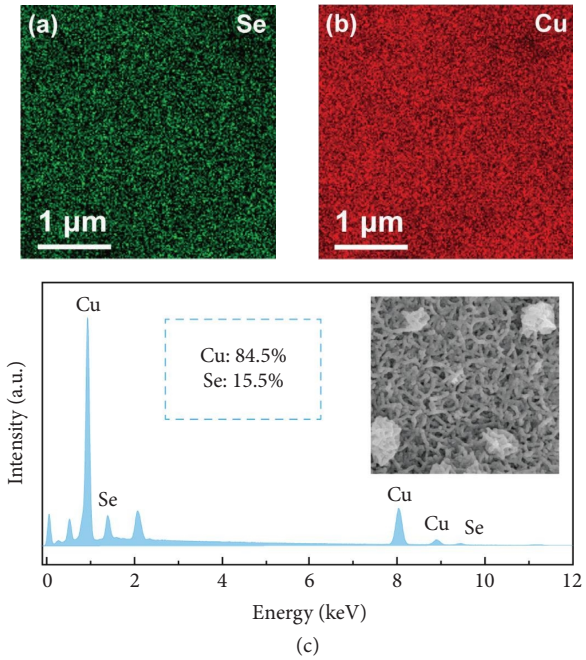

Figure 5: EDS mappings of (a) Se and (b) Cu, and (c) the compositional ratios of Se and Cu in the CuSe-based monolithic photocatalyst as derived from EDS mapping results.

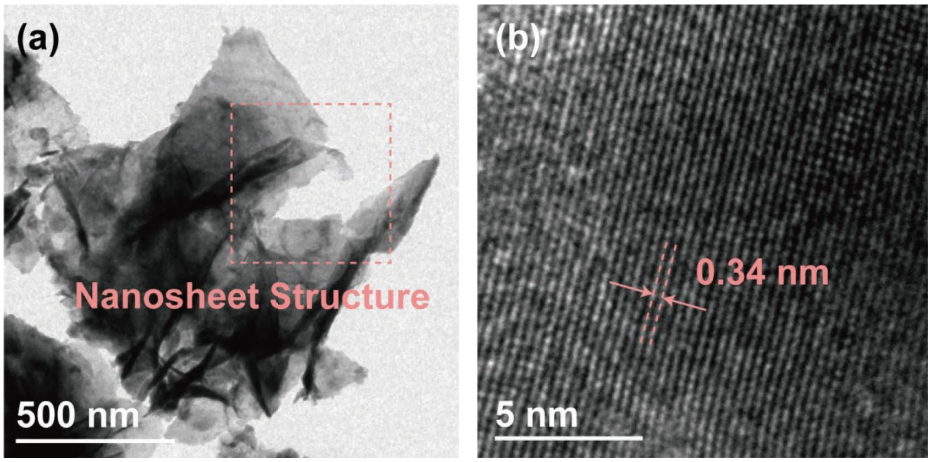

Figure 6: (a) TEM and (b) HRTEM images of the CuSe-based monolithic photocatalyst.

foam and well-dispersing them in ethanol, it was found that the rod-like nanoparticles were comprised of structured nanosheets. This observation agrees with the initial assumption that CuSe might grow along six energetically equivalent planes along the (100) directions, thus self-assembling into hexagonal phases that exclusively explored the (001) planes. Such a growth pattern would structure the CuSe into a nanosheet or nanoplanet that favors the exclusive exposure of a specific surface. Furthermore, based on the HRTEM image of the CuSe-based monolithic photocatalyst as prepared (as shown in Figure 6(b)), a lattice fringe of 0.34 nm was obtained for the nanosheet-structured material, which is attributed to the characteristic interlayer space between the (100) planes of CuSe [33]. Thus, based on the XRD, EDS, and HRTEM results, it is plausible enough to declare that the heterocomponents as formed on the surface of copper foam during the selenization process was CuSe in its hexagonal phase. Its growth preference made it shape as a nanosheet, which self-assembled into rod-like nanoparticles and fully covered the copper foam surface eventually. The monolithic structure and the adequate exposure of active sites might make the CuSe-based photocatalyst as synthesized an efficient and effective solution to organic dye pollution.

3.2. Photocatalytic Performance. After elucidating the chemical composition of the CuSe-based monolithic photocatalyst, MB was selected as a typical organic dye pollutant to test its photocatalytic performance. As shown in Figure 7, the adsorption of MB on CuSe-based monolith under dark condition was first ruled out. It was found that in the absence of light irradiation, the CuSe-based photocatalyst negligibly degraded MB, while, after the lamp was switched on, the MB concentration decreased rapidly. The results indicate that MB did not adsorb on the surface of CuSe-based monolith, and its degradation was primarily attributed to photooxidation. Besides, this work also compared the MB degradation performances of CuSe-based monolithic photocatalyst with powder CuSe, commercial P25, and commercial ZnO. As shown in Figure 8, the CuSe-based monolith obviously outperformed powder CuSe, commercial P25, and commercial ZnO in MB degradation. Compared to powder CuSe, the monolithic CuSe exposes more active sites due to its homogeneous distribution on the surface of copper foam. Compared to commercial TiO_2 and ZnO, CuSe possessed more favorable band gap that can effectively absorb both visible and ultraviolet light.

Then, this work tested the influence of copper foam density on the MB degradation performance of CuSe-based monolithic photocatalyst (as shown in Figure 9). When the density of copper foam equaled to 5 ppi, the CuSe-based monolithic photocatalyst as synthesized possessed a ~97% MB degradation efficiency within 120 min with the concentration of MB decreasing from 10 $mg{\cdot}L^{-1}$ to approximately 0.3 $mg{\cdot}L^{-1}$. By adjusting the density of the copper foam supporter to 10 and 20 ppi, it was found that the MB degradation performance of the CuSe-based monolithic photocatalyst was only negligibly

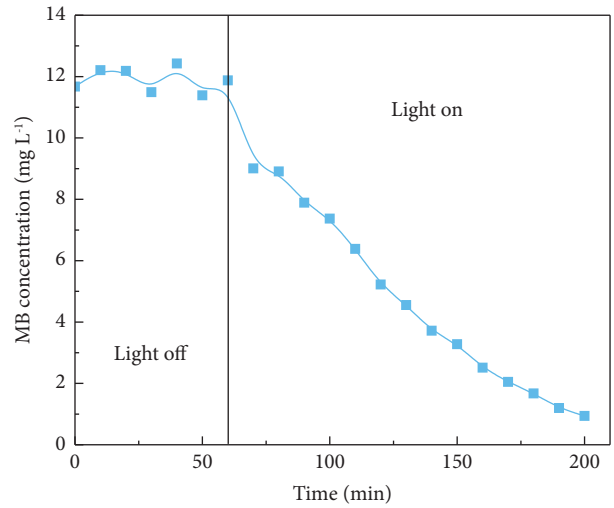

Figure 7: MB degradation performance of CuSe-based monolith under dark and light-irradiated conditions.

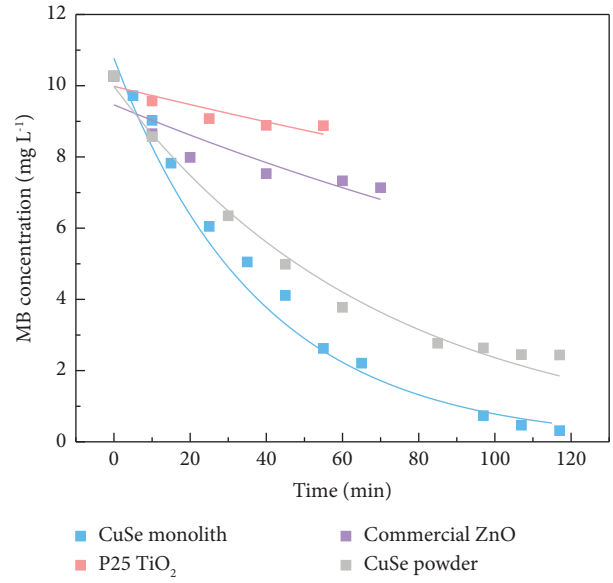

Figure 8: MB degradation performances of different photocatalysts.

affected. As shown, the CuSe-based monolithic photocatalysts supported on 10- and 20-ppi copper foam exhibited comparable MB degradation performances with that supported on 5-ppi copper foam, i.e., by decreasing the MB concentration from 10 $mg{\cdot}L^{-1}$ to around 0.3 $mg{\cdot}L^{-1}$ in a 120-min experiment. It is thus concluded that the density of copper foam is not a primary factor influencing the MB degradation performance of the CuSe-based monolithic photocatalyst. In the following experiments, the copper foam with a density of 10 ppi was used to test the effects of other influential factors.

The effects of photocatalyst dosage on the MB degradation performance of the CuSe-based monolithic photocatalyst are shown in Figure 10. As shown, when the dosage of the CuSe-based monolithic photocatalyst was two pieces,

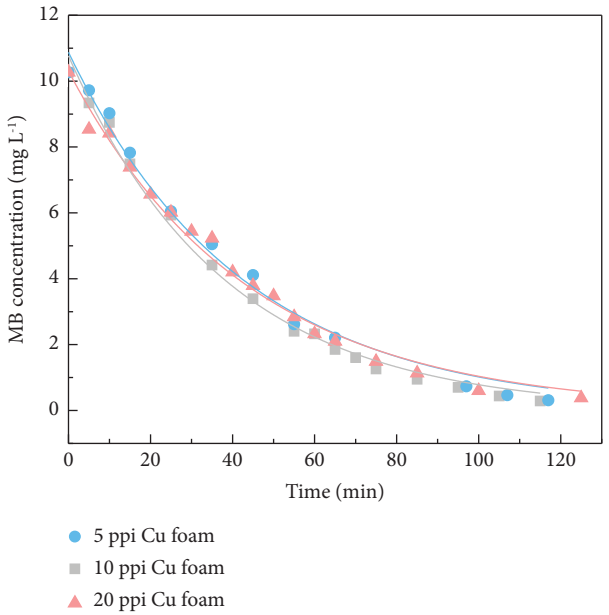

Figure 9: MB degradation performances of the CuSe-based monolithic photocatalyst loaded on Cu foams with different densities.

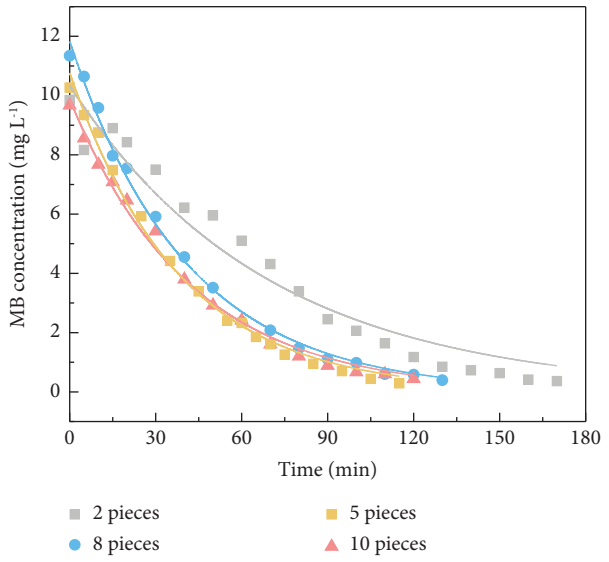

Figure 10: MB degradation performances of the CuSe-based monolithic photocatalysts with different dosages.

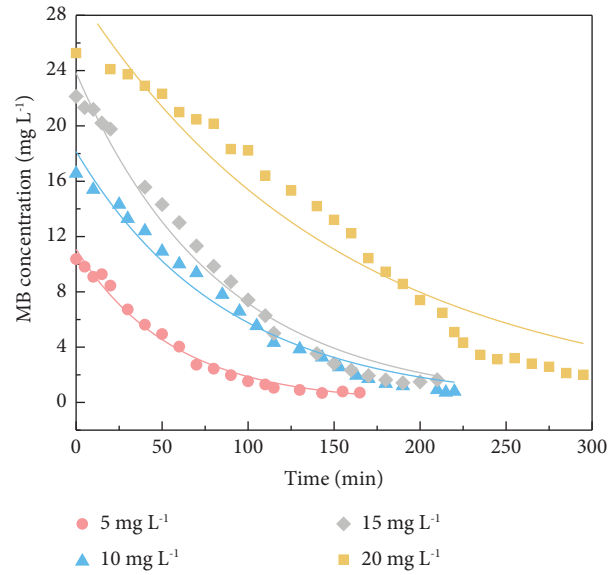

Figure 11: MB degradation performances of the CuSe-based monolithic photocatalysts with different initial MB concentrations.

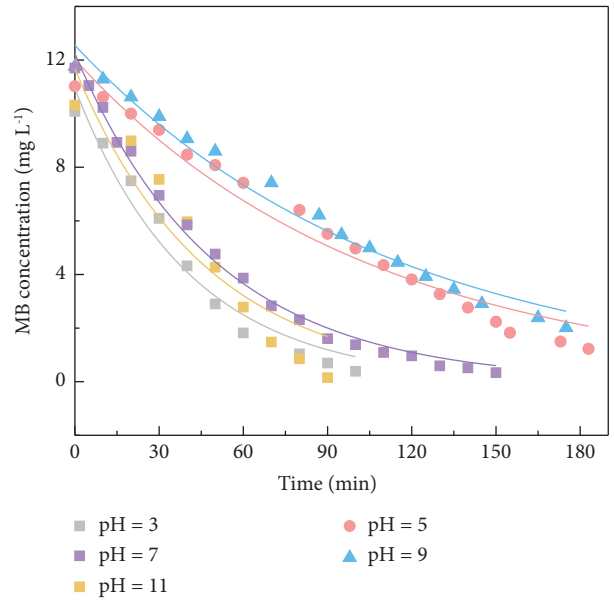

Figure 12: MB degradation performances of the CuSe-based monolithic photocatalysts under different pH conditions.

it achieved a ~96% MB degradation performance within 170 min, slightly inferior to the MB degradation performance of five-piece photocatalyst. Such inferiority may be attributed to the fact that extremely low dosage of the CuSe-based monolithic photocatalyst provided insufficient active sites for the degradation of MB. However, if the dosage of the CuSe-based monolithic photocatalyst increased to more than five pieces, i.e., eight and ten pieces, their MB degradation performances did not significantly improve compared to the five-piece scenario. This observation indicates that redundant active sites negligibly contributed to the improvement of MB degradation performance of the CuSe-based monolithic photocatalyst. In the case where the MB concentration equaled to 10 mg·L^{-1}, five-piece dosage of 1 × 1 × 1 cm CuSe-based monolithic photocatalyst was enough to achieve a relatively high MB degradation performance.

After identifying the optimal density and the photocatalyst dosage, the influence of MB concentration on the photocatalytic performance was that the CuSe-based monolithic photocatalyst was explored in the presence of 5, 10, 15, and 20 mg·L^{-1} of MB. As shown in Figure 11, after 150-min degradation, the CuSe-based monolithic photocatalyst could achieve a >98% MB degradation efficiency when the MB concentration equaled to 10 mg·L^{-1}.

Increasing the original concentration of MB to 15 mg·L^{-1} obviously extended the degradation time, i.e., in this case, five pieces of 10-ppi CuSe-based monolithic photocatalyst degraded more than 97% MB after 220 min. Similar performance of the CuSe-based monolithic photocatalyst was exhibited when the initial MB concentration was 20 mg·L^{-1}. Even when the MB concentration increased to 25 mg·L^{-1}, only five pieces of CuSe-based monolithic photocatalyst could reach a >90% MB degradation efficiency, which suggested that the CuSe-based monolithic photocatalyst as synthesized holds a great potential for practical degradation of MB from different industrial sources with fluctuated MB concentrations.

The influence of pH values on the MB degradation performance of the CuSe-based monolithic photocatalyst is shown in Figure 12. As shown, under a neutral pH value (pH = 7), the CuSe-based monolithic photocatalyst as synthesized exhibited moderate MB degradation performance. Slightly increasing or decreasing the pH value to 9 or 5 had an unobvious inhibitive effect on the MB degradation, i.e., the time used to achieve a >90% MB degradation efficiency was extended to more than 180 min. The adverse effect under the pH value of 5 might be attributed to acidic condition that made the photocatalyst positively charged, which compromised the adsorption of MB as a cationic component [34], while the detrimental influence under the pH value of 9 might be ascribed to the relatively high pH value that decreased the H^+ concentration in the MB solution, hence inhibiting the formation of HO_2^- ($H^+ + O_2 + 2e^- \longrightarrow HO_2^-$), a beneficial radical that facilitates MB photocatalytic degradation [35]. However, it was intriguingly found that, when the pH value further decreased from 5 to 3, the MB degradation performance of the CuSe-based monolithic photocatalyst was contrarily improved. This was because abundant H^+ ions in the MB solution favored the formation of HO^{2-} through a photocatalytic process [36]. Besides, a similar observation was also identified when further increasing the pH value from 9 to 11, which indicates that, under this circumstance, the adsorption of MB on the surface of the CuSe-based monolithic photocatalyst was significantly enhanced due to its negatively-charged nature [37]. Considering the adsorption of MB is the preliminary step for its photodegradation; the enhanced adsorption capacity towards MB is beneficial for its further conversion under light irradiation. Based on the abovementioned discussions, it is reasonable to declare that the CuSe-based monolithic photocatalyst as synthesized exhibited excellent compatibility and adaptability to harsh pH conditions, which did extend its application opportunities under practical scenarios. The TOC analysis shows that, within a 2-hour experiment, the TOC removal efficiency reached >70%, which demonstrates that both decolorization and mineralization played functional roles during the degradation of MB, while the mineralization played the dominant role (as shown in Figure 13).

Finally, to justify the cost-effectiveness of the CuSe-based monolithic photocatalyst, a recycling experiment was conducted to determine the MB degradation performances in different cycles with the same batch of photocatalyst. As

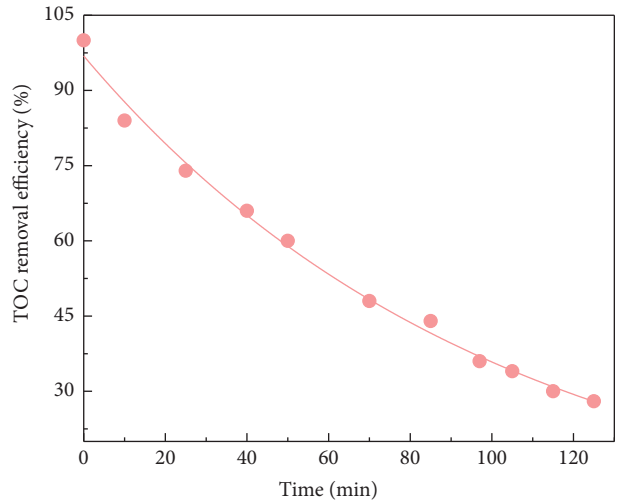

Figure 13: TOC removal efficiency of the CuSe-based monolithic photocatalyst.

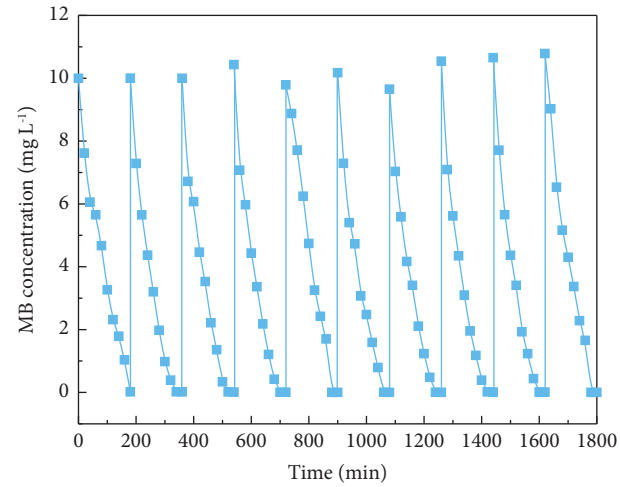

Figure 14: MB degradation performances of the CuSe-based monolithic photocatalysts for several cycles.

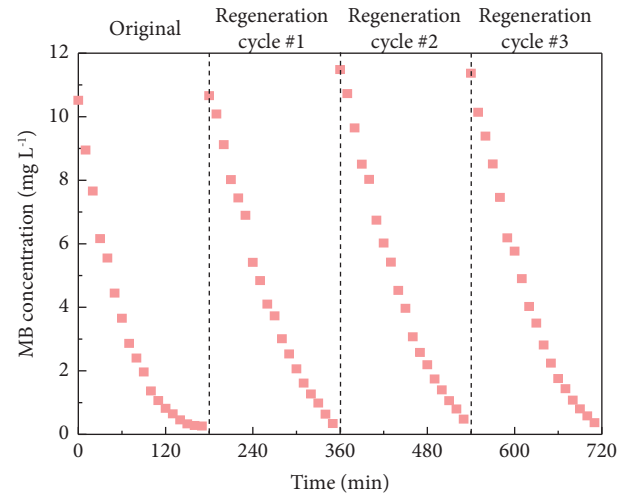

Figure 15: MB degradation performances of regenerated CuSe-based monolithic photocatalysts.

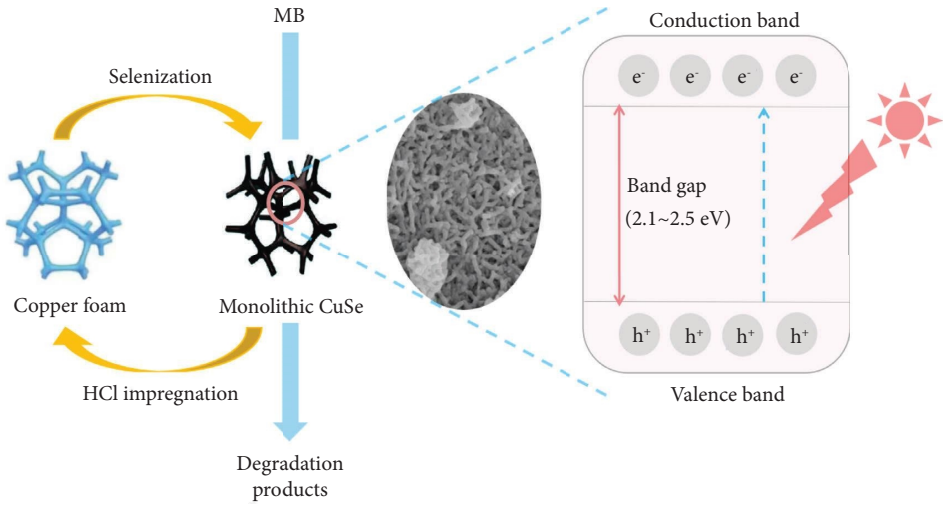

Figure 16: Diagrammatical illustration of the MB degradation on the CuSe-based monolithic photocatalyst.

shown in Figure 14, in a cyclic experiment, the CuSe-based monolithic photocatalyst exhibited comparable MB degradation performances for ten continuous cycles, which indicates that the photocatalyst is relatively stable in degrading MB. As shown in Figure 15, in the regeneration experiments, it could be found that the MB degradation performances of regenerated CuSe-based monolithic photocatalyst negligibly declined compared to the original one. The regenerated CuSe-based monolithic photocatalyst also exhibited >95% MB degradation efficiency within a 3 hour experiment, which suggests that the HCl-impregnation followed by reselenization process can effectively regenerate the deactivated photocatalyst. From these perspectives, the CuSe-based monolithic photocatalyst possessed a relatively decent recyclability and reusability in the photocatalytic degradation of MB. Such favorability will further save the operational cost if the CuSe-based monolithic photocatalyst was used as alternatives to traditional powdery photocatalysts for MB removal from dye-polluted industrial effluents. The performance tests involving the influence of copper foam density, photocatalyst dosage, MB concentration, pH value, and cyclic number fully demonstrate the possibility to progressively extend the research and discussion on the CuSe-based monolithic photocatalyst in the future (as briefly illustrated in Figure 16).

4. Conclusions

In conclusion, this work primarily developed a method to prepare a CuSe-based monolithic photocatalyst as an efficient alternative to traditional powdery ones. The CuSe-based photocatalyst as synthesized well-kept its monolithic structure during the photocatalytic reaction process due to the maintenance of the copper skeleton after selenization. Besides, the surface of the monolithic photocatalyst fully covered by CuSe ensured that it exhibited decent performance towards MB degradation. In particular, activity test results showed that the CuSe-based monolithic photocatalyst as prepared could successfully achieve a ~97% MB degradation efficiency. Notably, this efficient photocatalyst also exhibited resistance to harsh pH conditions, i.e., under the pH values of both 3 and 11, the MB degradation performance of the CuSe-based monolithic photocatalyst was further improved compared to the performance under a pH value of 7. These outstanding performances support that the CuSe-based monolithic photocatalyst may be a promising alternative to traditional powdery photocatalysts to ensure the recyclability and extend the applicability of the photocatalytic techniques for organic dye removal and industrial effluent cleaning.

Data Availability

The data used to support the findings of this study are available from the corresponding author upon request.

Conflicts of Interest

The authors declare that they have no conflicts of interest.

Acknowledgments

This work was supported by the College Students' Innovative Entrepreneurial Training Plan Program of China (No. S2022105330951) and the Open Sharing Fund for the Large-Scale Instruments and Equipments of Central South University.

References

[1] S. Moosavi, C. Lai, S. Gan, G. Zamiri, O. Akbarzadeh Pivehzhani, and M. Johan, "Application of efficient magnetic particles and activated carbon for dye removal from wastewater," *ACS Omega*, vol. 5, no. 33, pp. 20684–20697, 2020.

[2] M. Din, R. Khalid, J. Najeeb, and Z. Hussain, "Fundamentals and photocatalysis of methylene blue dye using various nanocatalytic assemblies- a critical review," *Journal of Cleaner Production*, vol. 298, Article ID 126567, 2021.

[3] H. Lachheb, E. Puzenat, A. Houas et al., "Photocatalytic degradation of various types of dyes (alizarin S, crocein orange G, methyl red, Congo red, methylene blue) in water by

UV-irradiated titania," *Applied Catalysis B: Environmental*, vol. 39, no. 1, pp. 75–90, 2002.

[4] L. Xie, X. Jiang, and J. Yu, "A novel low-cost bio-sorbent prepared from crisp persimmon peel by low-temperature pyrolysis for adsorption of organic dyes," *Molecules*, vol. 27, no. 16, p. 5160, 2022.

[5] L. Ma, C. Jiang, Z. Lin, and Z. Zou, "Microwave-hydrothermal treated grape peel as an efficient biosorbent for methylene blue removal," *International Journal of Environmental Research and Public Health*, vol. 15, no. 2, p. 239, 2018.

[6] A. Habibi and K. Narimani Rad, "Mass transfer effects on biodegradation of methylene blue by immobilized cell in a packed bed bioreactor," *Asia-Pacific Journal of Chemical Engineering*, vol. 14, no. 1, Article ID e2269, 2019.

[7] A. Bhardwaj, S. Nag, K. Hussain, P. Pandey, and J. Babu, "Effect of temperature and fly ash content on the catalytically pyrolyzed rice straw biochar-fly ash composites for methylene blue adsorption," *Asia-Pacific Journal of Chemical Engineering*, vol. 17, no. 6, Article ID e2828, 2022.

[8] K. Naseem, Z. Farooqi, M. Ur Rehman et al., "A systematic study for removal of heavy metals from aqueous media using Sorghum bicolor: an efficient biosorbent," *Water Science and Technology*, vol. 77, no. 10, pp. 2355–2368, 2018.

[9] W. Pronk, A. Ding, E. Morgenroth et al., "Gravity-driven membrane filtration for water and wastewater treatment: a review," *Water Research*, vol. 149, pp. 553–565, 2019.

[10] Y. Ho, S. Chua, and F. Chong, "Coagulation-flocculation technology in water and wastewater treatment," *Handbook of Research on Resource Management for Pollution and Waste Treatment*, pp. 432–457, IGI Global, Pennsylvania, PA, USA, 2020.

[11] A. Manivel, G. Lee, C. Chen et al., "Synthesis of MoO_3 nanoparticles for azo dye degradation by catalytic ozonation," *Materials Research Bulletin*, vol. 62, pp. 184–191, 2015.

[12] M. Din, J. Najeeb, Z. Hussain, R. Khalid, and G. Ahmad, "Biogenic scale up synthesis of ZnO nano-flowers with superior nano-photocatalytic performance," *Inorganic and Nano-Metal Chemistry*, vol. 50, no. 8, pp. 613–619, 2020.

[13] J. Wang and M. Zhao, "Economic impacts of ISO 14001 certification in China and the moderating role of firm size and age," *Journal of Cleaner Production*, vol. 274, Article ID 123059, 2020.

[14] W. Wang, T. An, G. Li, Y. Li, J. C. Yu, and P. Wong, "Free-standing red phosphorous/silver sponge monolith as an efficient and easily recyclable macroscale photocatalyst for organic pollutant degradation under visible light irradiation," *Journal of Colloid and Interface Science*, vol. 518, pp. 130–139, 2018.

[15] X. Li, J. Yu, and M. Jaroniec, "Hierarchical photocatalysts," *Chemical Society Reviews*, vol. 45, no. 9, pp. 2603–2636, 2016.

[16] S. Sharma and S. Basu, "Fabrication of centimeter-sized Sb_2S_3/SiO_2 monolithic mimosa pudica nanoflowers for remediation of hazardous pollutants from industrial wastewater," *Journal of Cleaner Production*, vol. 280, Article ID 124525, 2021.

[17] Z. Shen, Q. Zhang, C. Yin et al., "Facile synthesis of 3D flower-like mesoporous Ce-ZnO at room temperature for the sunlight-driven photocatalytic degradations of RhB and phenol," *Journal of Colloid and Interface Science*, vol. 556, pp. 726–733, 2019.

[18] M. Sabri, A. Habibi-Yangjeh, H. Chand, and V. Krishnan, "Activation of persulfate by novel TiO_2/FeOCl photocatalyst under visible light: facile synthesis and high photocatalytic performance," *Separation and Purification Technology*, vol. 250, Article ID 117268, 2020.

[19] S. Zarezadeh, A. Habibi-Yangjeh, and M. Mousavi, "Fabrication of novel ZnO/BiOBr/C-Dots nanocomposites with considerable photocatalytic performances in removal of organic pollutants under visible light," *Advanced Powder Technology*, vol. 30, no. 6, pp. 1197–1209, 2019.

[20] A. Phuruangrat, A. Maneechote, P. Dumrongrojthanath, N. Ekthammathat, S. Thongtem, and T. Thongtem, "Effect of pH on visible-light-driven Bi2WO6 nanostructured catalyst synthesized by hydrothermal method," *Superlattices and Microstructures*, vol. 78, pp. 106–115, 2015.

[21] N. Ekthammathat, S. Thongtem, T. Thongtem, and A. Phuruangrat, "Characterization and antibacterial activity of nanostructured ZnO thin films synthesized through a hydrothermal method," *Powder Technology*, vol. 254, pp. 199–205, 2014.

[22] W. Ali, H. Ullah, A. Zada et al., "Synthesis of TiO_2 modified self-assembled honeycomb ZnO/SnO_2 nanocomposites for exceptional photocatalytic degradation of 2,4-dichlorophenol and bisphenol A," *The Science of the Total Environment*, vol. 746, Article ID 141291, 2020.

[23] W. Ahmad, M. Basit, M. Khan, I. Ali, and T. Park, "Superior atomic layer deposition of conformal ZnO shell on spherical SiO_2 particles for enhanced photocatalytic activity," *Physica E: Low-Dimensional Systems and Nanostructures*, vol. 124, Article ID 114308, 2020.

[24] M. Xiao, L. Zhang, B. Luo et al., "Molten-salt-mediated synthesis of an atomic nickel Co-catalyst on TiO_2 for improved photocatalytic H_2 evolution," *Angewandte Chemie*, vol. 132, no. 18, pp. 7297–7301, 2020.

[25] R. Kavitha and S. Kumar, "A review on plasmonic Au-ZnO heterojunction photocatalysts: preparation, modifications and related charge carrier dynamics," *Materials Science in Semiconductor Processing*, vol. 93, pp. 59–91, 2019.

[26] G. Karmakar, A. Tyagi, A. Wadawale et al., "Accessing photoresponsive copper selenide nanomaterials and thin films through tetranuclear Cu (I) pyridylselenolate cluster," *Journal of Materials Science*, vol. 55, no. 32, pp. 15439–15453, 2020.

[27] I. Shitu, K. Katibi, L. Taura et al., "X-ray diffraction (XRD) profile analysis and optical properties of Klockmannite copper selenide nanoparticles synthesized via microwave assisted technique," *Ceramics International*, vol. 49, no. 8, pp. 12309–12326, 2023.

[28] D. Winn and M. Doherty, "Modeling crystal shapes of organic materials grown from solution," *AIChE Journal*, vol. 46, no. 7, pp. 1348–1367, 2000.

[29] Z. Yang, H. Li, J. Yang et al., "Nanosized copper selenide functionalized zeolitic imidazolate framework-8 (CuSe/ZIF-8) for efficient immobilization of gas-phase elemental mercury," *Advanced Functional Materials*, vol. 29, no. 17, Article ID 1807191, 2019.

[30] S. Lu, Z. Wang, H. Yan et al., "High rate and cycling stable Li metal anodes enabled with aluminum-zinc oxides modified copper foam," *Journal of Energy Chemistry*, vol. 41, pp. 87–92, 2020.

[31] Y. Li, S. Chang, X. Liu et al., "Nanostructured CuO directly grown on copper foam and their supercapacitance performance," *Electrochimica Acta*, vol. 85, pp. 393–398, 2012.

[32] W. Lu, Y. Sun, H. Dai et al., "Direct growth of pod-like Cu_2O nanowire arrays on copper foam: highly sensitive and efficient nonenzymatic glucose and H_2O_2 biosensor," *Sensors and Actuators B: Chemical*, vol. 231, pp. 860–866, 2016.

[33] X. Wu, X. Huang, J. Liu et al., "Two-dimensional CuSe nanosheets with microscale lateral size: synthesis and

template-assisted phase transformation," *Angewandte Chemie International Edition*, vol. 53, no. 20, pp. 5083–5087, 2014.

[34] F. Azeez, E. Al-Hetlani, M. Arafa et al., "The effect of surface charge on photocatalytic degradation of methylene blue dye using chargeable titania nanoparticles," *Scientific Reports*, vol. 8, no. 1, p. 7104, 2018.

[35] Y. Seo and S. Oh, "Controlling the recombination of electron-hole pairs by changing the shape of ZnO nanorods via sol-gel method using water and their enhanced photocatalytic properties," *Korean Journal of Chemical Engineering*, vol. 36, no. 12, pp. 2118–2124, 2019.

[36] X. Lin, F. Huang, W. Wang, and K. Zhang, "A novel photocatalyst $BiSbO_4$ for degradation of methylene blue," *Applied Catalysis A: General*, vol. 307, no. 2, pp. 257–262, 2006.

[37] Q. Xiao, J. Zhang, C. Xiao, and X. Tan, "Photocatalytic decolorization of methylene blue over $Zn_{1-x}Co_xO$ under visible light irradiation," *Materials Science and Engineering: B*, vol. 142, no. 2-3, pp. 121–125, 2007.